Aeroelastic Coupling Effects in Globally Unstable Transonic Wing Flow

Panagiotis Belesiotis–Kataras* and Sebastian Timme†
University of Liverpool, Liverpool, L69 3GH, United Kingdom

This work concerns the phenomenon of shock buffet and its mutual interaction with the flexible wing structure. The latter aspect is key to our contribution, since, even though renewed interest in edge-of-the-envelope flow unsteadiness can be observed in recent years, the multidisciplinary aeroelastic interaction is typically overlooked. Previous work by Timme [1] applied stability theory to a large aircraft wing, specifically the NASA Common Research Model, to reveal a global instability linked to shock buffet. Herein, we expand upon that work by adding the dimension of wing vibration to scrutinise its impact on the flow unsteadiness. We consider fluid-structure interaction solving the unsteady Reynolds-averaged Navier–Stokes equations with an industry-grade computational fluid dynamics solver to model the aerodynamics and a modal structural model of the actual wind-tunnel geometry to describe the flexible wing. Our focus experimental flow condition is a reference free-stream Mach number of 0.85 with a chord Reynolds number of 5×10^6 and a supercritical angle of attack of 3.75°. Results show that the initial aerodynamic unsteadiness, when started from a well converged static aeroelastic solution (validated with wind-tunnel data), is nearly independent of the presence of the flexible wing structure as long as the amplitudes are small. Indeed wing vibration follows the dominant shock-buffet excitation. Once transitioned into the non-linear aerodynamic regime (while noting that at the time of writing a longer time history is still required), most of the structural degrees-of-freedom are active close to their respective natural frequencies and also within the shock-buffet frequency range. An aeroelastic global stability analysis presented in our companion paper [2] has revealed that several of these modes become unstable due to the fluid-structure coupling. Overall the impact of the flexible wing results in lower amplitudes in integrated aerodynamic coefficients with a broader frequency content peaking around the first bending frequencies and the shock-buffet frequency range, which is in contrast to the rigid (yet statically deformed) wing where the shock-buffet excitation clearly dominates.

I. Introduction

Designing the wings of the future is a challenge faced by aerodynamicists in an effort to satisfy the toughest requirements of the aviation industry for faster, safer and more sustainable aircraft. Focussing on civil air transport, the variety of detrimental phenomena encountered in high-speed edge-of-the-envelope flight poses great design limitations in pushing these boundaries. Transonic shock buffet is one such flow phenomenon emerging from the strong interaction of shock waves and separated boundary layers and producing a self-excited and self-sustained unsteadiness. It imposes a drag penalty along with an unwanted structural excitation (called buffeting) that goes hand in hand with an increase in fuel consumption and a general degradation of the aircraft handling qualities and passenger comfort. Since its first observation over six decades ago [3], shock buffet has attracted considerable interest, and numerous studies have looked into its mechanisms both for two-dimensional aerofoils and finite wings. Nevertheless, the multidisciplinary physics of shock buffet, especially on flexible wings, remains elusive. As a result, design constraints are imposed to satisfy a 30% safety margin to the point where structural vibration and buffeting is observed [4]. Hence, a thorough understanding of the phenomenon is an important step in designing and optimising future wings.

Following the analysis of experimental studies on aerofoils [5], it was demonstrated that two-dimensional shock buffet has a characteristic shedding frequency that is more or less independent of geometry [6]. It was also shown that the characteristics change when dealing with a finite wing, as the typical frequencies shift to higher values by up to an order of magnitude and become broadband (i.e. a Strouhal number range of 0.06 to 0.08 has been reported for aerofoils, while it is 0.2 to 0.7 for finite swept wings). The strong correlation between the buffet dynamics observed on aerofoils

*PhD Student, School of Engineering, P.Belesiotis-Kataras@liverpool.ac.uk
†Senior Lecturer, School of Engineering, Sebastian.Timme@liverpool.ac.uk. Member AIAA.

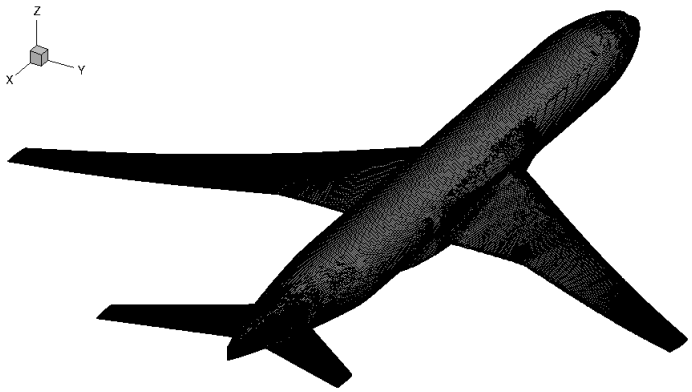

Fig. 1 Illustration of NASA CRM full-span geometry and surface mesh.

and straight wings implied that the main reason behind these discrepancies can be found in the sweep angle [7], which exacerbated the flow unsteadiness due to the three-dimensional effects that become dominant for sweep angles of 20° and above. It is important to point out here that modern large aircraft have a typical sweep angle around 30°. Pronounced shock-wave/boundary-layer interaction taking place beyond shock-buffet onset gives rise to aeroelastic phenomena due to the inevitable flexibility of large aircraft wings. Importantly, the shock-buffet frequency range coincides with higher-frequency structural modes of those aircraft models [8], which warrants a multidisciplinary approach.

While most numerical [9–13] and experimental [14–19] studies shed light on the mechanisms that govern the fluid part of the phenomenon assuming rigid aerofoils and wings, the literature in which the details of the coupled fluid-structure system, specifically for finite wings, are scrutinised remains limited. Studies on both single- and two-degrees-of-freedom (pitch and pitch-and-heave, respectively) aerofoils investigated the response of the aeroelastic system subjected to an unsteady periodic flow, specifically shock buffet. It was shown that for certain combinations of oscillation amplitude and structural frequencies (with the amplitude above some threshold and frequency close to the characteristic aerodynamic frequency), a lock-in phenomenon was observed where the frequency of the oscillating flow field would synchronise with that of the structural system. Due to the asymmetric nature of the lock-in boundaries, skewed towards higher frequencies, the idea that a pure resonance mechanism is responsible, previously observed for an elastically suspended cylinder in the form of vortex-induced vibration [20, 21], was ruled out [22–24]. Linear stability analysis utilising a reduced-order model of a single-degree-of-freedom aerofoil showed that the coupling of the two systems results in coupled fluid-mode flutter [25]. Similarly, in [26] it was demonstrated that the mutual interaction of the fluid and structure destabilised an otherwise stable fluid mode, hence lowering the buffet onset point, compared with results for fixed, non-moving fluid boundaries. Experimental studies on a flexible finite swept wing undergoing shock-wave/boundary-layer interaction at high-speed conditions revealed a strong response of the aeroelastic system in the frequency of the oscillating flow field instead of a structural eigenfrequency [27].

Other experimental work on finite swept wings using state-of-the-art dynamic pressure sensitive paint as well as conventional instrumentation has helped to elucidate the complex mechanisms of transonic shock buffet by identifying two distinct phenomena [28]. Using both dynamic mode decomposition and proper orthogonal decomposition for data analysis, one of those phenomena was what is widely recognised as shock buffet, associated with localised outboard-running perturbations beyond the onset of global unsteadiness, whereas the second lower-frequency behaviour described large-scale inboard-running shock unsteadiness observed even in subcritical conditions. Granted that only the former has been linked to an unstable global mode [1], there has not been a clear explanation regarding the latter. This bears a resemblance to the findings in prior work where a lower-frequency mechanism was excited by harmonic structural forcing both in the presence and absence of the global instability [11, 29].

Herein we investigate the influence of structural coupling on the dynamic response of an aircraft wing in a flow condition beyond shock-buffet onset where the flow is globally unstable. A static aeroelastic simulation is carried out initially to obtain the statically deformed wing shape at the given flow condition. Using this as a starting point, two time-marching simulations, namely fluid-only and coupled fluid-structure, are carried out to allow a quantitative discussion of the influence of the flexible wing on the shock-buffet dynamics, and vice versa. The test case discussed in this work is introduced in Section II. Then, the numerical approach is outlined briefly in Section III before presenting the simulation results and contemplating the main findings in Section IV.

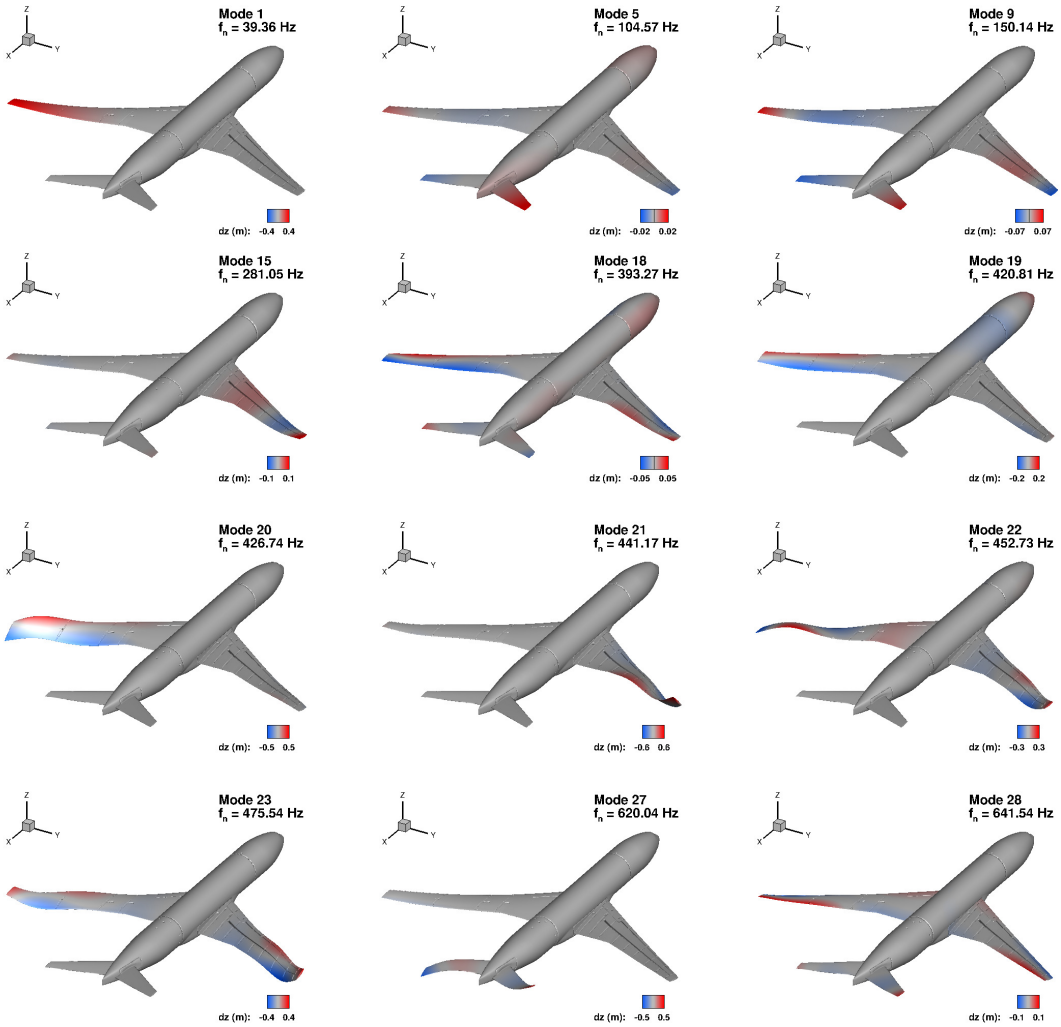

Fig. 2 Representative normal mode shapes from wind-off vibration analysis, with mass-normalised eigenvectors scaled by a factor of 0.1 for visualisation purposes. Surface colours describe modal deformation in z-direction.

II. Large Aircraft Wing Test Case

The chosen test case is the NASA Common Research Model (CRM) in the wing/body/horizontal-tail configuration (with 0° tail setting angle) scaled to wind-tunnel dimensions. The wing has a quarter-chord sweep angle of 35°, a reference area of 0.280 m^2, a taper ratio of 0.275, an aerodynamic mean chord of 0.189 m, a semi-span of 0.793 m and an aspect ratio of 9 [30]. This wing geometry, shown in fig. 1, has been studied by the authors in the past in the context of linearised aerodynamics analysis in the shock-buffet regime investigating both forced structural excitation (through a synthetic torsion mode) and aerodynamic stability [1, 31]. For the current fluid-structure coupled simulation, the structural modes of vibration were obtained from the finite-element model* of the underlying wind-tunnel geometry. Overall, 30 modes of lowest frequency were retained for the current study. A few representative modal shapes can be seen in figure 2, where the mass-normalised eigenvectors have been scaled by a factor of 0.1 for visualisation purposes only, due to the otherwise excessive deformations.

An unstructured mesh was generated for the half-span simulations in [1], using the Solar mesh generator and following industry accepted guidelines. Herein, once mirrored with respect to the fuselage centre plane, the full-span mesh is composed of approximately 12×10^6 points. The surface mesh is shown in fig. 1, while a spherical far-field boundary is applied at a distance of approximately 100 times the semi-span of the model.

*found at https://commonresearchmodel.larc.nasa.gov/

III. Methodology

Governing Equations

For the fluid domain, the governing equations are the Reynolds-averaged Navier–Stokes equations along with the negative Spalart–Allmaras one-equation turbulence model for closure. The state vector containing the conservative variables is defined as $\boldsymbol{w} = [\rho, \rho u, \rho v, \rho w, \rho E, \rho\check{\nu}]^T$ with ρ as the density, (u, v, w) as the Cartesian velocity components, E as the energy and $\check{\nu}$ as the primitive working variable of the turbulence model. The governing equations can be written in semi-discrete form as

$$\frac{\mathrm{d}M\boldsymbol{w}}{\mathrm{d}t} = -\boldsymbol{R}(\boldsymbol{w}, \boldsymbol{x}, \dot{\boldsymbol{x}}) \tag{1}$$

where M is the matrix containing the discrete control volumes and $\boldsymbol{R}$ is the residual vector containing the spatial discretisation. The dual time-stepping method with second-order backward differentiation formula is given through

$$\boldsymbol{R}^* = \boldsymbol{R}(\boldsymbol{w}, \boldsymbol{x}, \dot{\boldsymbol{x}}) + \frac{3(M\boldsymbol{w})^{n+1} - 4(M\boldsymbol{w})^n + (M\boldsymbol{w})^{n-1}}{2\Delta t} \tag{2}$$

where Δt is the time step. The discrete control volumes are time-dependent observing the geometric conservation law.

For the structural system, the equations of motion in modal coordinates $\boldsymbol{q}$ are

$$\Phi^T M \Phi \ddot{\boldsymbol{q}} + \Phi^T K \Phi \boldsymbol{q} = \Phi^T \boldsymbol{f}_a \tag{3}$$

where $\Phi = [\boldsymbol{\phi}_1, \boldsymbol{\phi}_2, \ldots, \boldsymbol{\phi}_m]$ is the matrix containing the m leading normal mode shapes based on frequency. The physical structural coordinates $\boldsymbol{x}_s$ relate to the mode shapes and modal amplitudes as $\boldsymbol{x}_s(t) = \Phi\boldsymbol{q}(t)$. Also, the term on the right-hand side in eq. (3) denotes the generalised aerodynamic force vector. No structural damping is assumed.

Simulation Tools

The unstructured finite-volume solver TAU, developed by the German Aerospace Center (DLR) and widely used in both European industry and academia, is chosen for the flow simulations. Second-order spatial discretisation uses the standard central scheme with matrix artificial dissipation. The negative Spalart–Allmaras one-equation model (assuming fully turbulent flow) is discretised with a first-order upwind scheme. This choice is based on observing unsteadiness with a similar setup in previous studies [13]. The Green–Gauss theorem is used for reconstructing the gradients of the flow variables where needed. An implicit backward Euler solver converges the non-linear flow equations to steady state. Local time-stepping and geometric multigrid on three grid levels are employed to accelerate convergence. For the fluid-only unsteady simulation (starting from the static aeroelastic solution, described below, and imposing the frozen geometry at the equilibrium point), Courant–Friedrichs–Lewy numbers of 20 for the finest grid level and 5 for the coarser grid levels are chosen. Dual time-stepping with the second-order backward differentiation formula is used for integration in time, as shown in eq. (2). A physical time-step size of $\Delta t = 2$ μs was applied, sufficient for the expected frequencies in the dynamic system. The aerodynamic state is then evaluated for each real time step by iterating the pseudo residual $\boldsymbol{R}^*$ to a steady state with a minimum of 50 inner iterations per time step and a relative Cauchy convergence criterion of 10^{-8} on the drag coefficient.

FlowSimulator is used for the fluid-structure coupled simulations. This software enables computational fluid dynamics enhanced multidisciplinary simulations on massively parallel computing systems while providing a plug-in environment where different flow solver tools and developer scripts can be utilised [32]. For the static aeroelastic simulation that is performed to obtain the wing deformation balancing the aerodynamic loads according to the given conditions, specifically solving $\Phi^T K \Phi \boldsymbol{q} = \Phi^T \boldsymbol{f}_a$, both fluid and structural system are converged to an equilibrium in a maximum of 40 outer coupling iterations, with up to 100 iterations of the flow solver per outer iteration. This solution is used as the starting point for the dynamic fluid-structure coupled simulation. For each real time step, up to five coupling iterations are allowed each with 50 inner iterations of the flow solver and the Newmark-beta integration scheme applied for the structural update. Convergence is assessed based on the norm of the relative change in the generalised aerodynamic force vector between iterations. The tolerance is set to 10^{-3} and a minimum of three coupling iterations is always performed. Consistent with the fluid-only simulation, a physical time-step size of $\Delta t = 2$ μs was chosen.

IV. Results

Following previous work [1, 31], the focus in this study is on a free-stream Mach number of 0.85 and the Reynolds number (based on the mean aerodynamic chord) is 5×10^6. For the purpose of converting frequencies to and

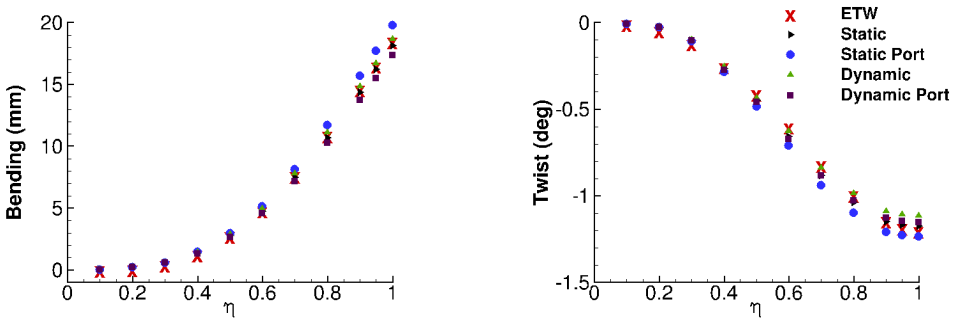

Fig. 3 Bending and twist deformation plots at $\alpha = 3.75°$, comparing data from simulation and wind-tunnel measurements in European Transonic Windtunnel (ETW) for eleven non-dimensional spanwise stations η on both port and starboard wings. Experimental data were interpolated from angles of attack $\alpha = 3.0°$ and $4.0°$ [33].

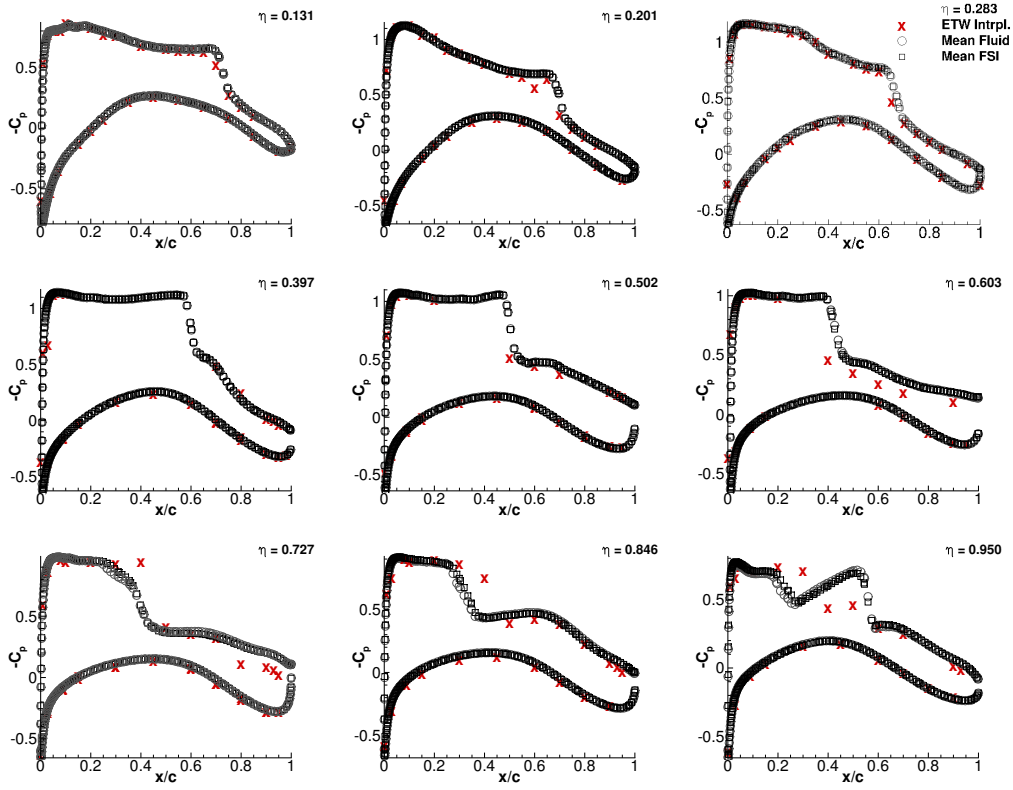

Fig. 4 Surface pressure coefficient C_p at $\alpha = 3.75°$, comparing simulation and wind-tunnel test results for nine spanwise stations of starboard wing. Fluid-only and fluid-structure interaction (FSI) data are time-averaged signals from non-linear regime.

from non-dimensional form, we state the reference velocity as $281.5\,\mathrm{ms}^{-1}$. The focus angle of attack herein is the supercritical $\alpha = 3.75°$. Reynolds-averaged Navier–Stokes simulations on a rigid (yet statically deformed according to data from the underlying test campaign in the European Transonic Windtunnel) geometry have shown that self-sustained flow unsteadiness occurred for angles of attack above (and including) $\alpha = 3.70°$. This unsteadiness was related to a global instability through an eigenvalue crossing into the unstable half plane for this critical angle of attack at a Strouhal number of approximately $St = 0.39$ (corresponding to a frequency of 580 Hz) [1]. The wind-off structural frequencies of the normal modes retained for the coupled simulation cover a range of 40 Hz to 680 Hz. For the highest structural mode, the chosen time-step size of $\Delta t = 2\ \mu$s gives more than 700 physical time steps per oscillation cycle.

We start by presenting some basic validation with respect to measurements from the wind-tunnel campaign, including deformation and pressure data. Figure 3 shows deformation data, specifically wing bending and twist taken at 50%

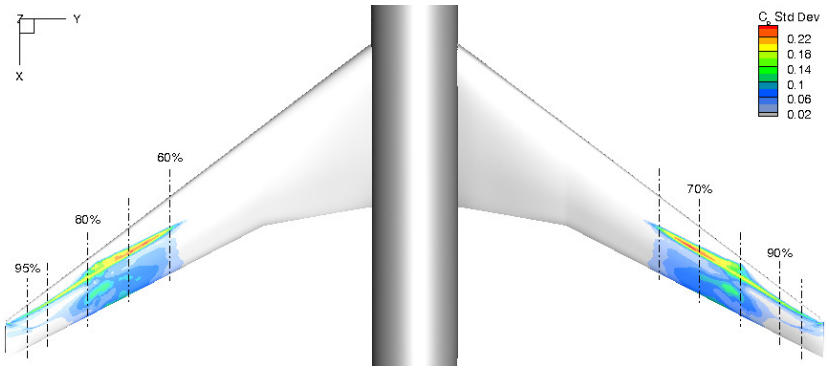

Fig. 5 Standard deviation of surface pressure coefficient for rigid (yet statically deformed) (on the left) and flexible wing (right). Both wings depict the starboard wing (whereby the rigid wing has been mirrored for visualisation purposes).

local chord along the non-dimensional span coordinate η (made dimensionless using the semi-span length), comparing experimental data, using stereo pattern tracking via markers distributed on the wing surface, and numerical data from both the static and dynamic aeroelastic simulations, whereby the latter are the time-averaged values from the non-linear regime of the signal (to be discussed below). Note that the experiment measured the deformation at angles of attack $\alpha = 3.0^\circ$ and 4.0°, hence interpolation was required as described in [33]. Three observations can easily be made. First, the numerical results reveal a minor asymmetry between the port and starboard wing, effectively resulting from the high-fidelity finite-element model of the actual wind-tunnel geometry which includes various details of asymmetric cut-outs for accommodating the instrumentation, etc. (note the subtle surface features in figure 2 in this regard). Second, there are clear differences between the static and time-averaged dynamic deformation. Third, the time-averaged dynamic deformation of the simulation agrees better with the experimental data overall, in particular for the port wing, which makes sense in that also the experimental data relate to some mean deformation. Figure 4 describes the corresponding surface pressure coefficient C_p at nine spanwise stations. The numerical data include results from both time-averaged fluid-only and fluid-structure interaction simulations. Again we can easily make three observations. First, the experimental pressure sensors are rather sparse in the mid semi-span stations. This has been discussed previously [1, 34]. Second, the differences in the time-averaged pressures from the fluid-only and fluid-structure coupled simulation are rather small, almost indistinguishable, which does not seem unreasonable considering the proximity of the simulations to the shock-buffet onset angle of attack. Third, while the level of agreement between simulation and experiment is acceptable overall, discrepancies are also noticeable, particularly for the stations outboard of approximately $\eta = 0.603$. In previous work, this was the region where the shock-buffet unsteadiness was located [1], suggesting that better simulations, e.g. through more advanced turbulence modelling and eddy-resolving approaches, are needed in general. Having said this, our simulations are on a par with various other state-of-the-art solvers [34].

Figure 5 shows the standard deviation of the surface pressure coefficient, again noting that at the time of writing a longer unsteady signal was still required. The figure presents the results on the starboard wing for both the fluid-only and fluid-structure coupled simulations. The fluid-only data have been mirrored for visualisation purposes only. High levels of an outboard-running (identified from instantaneous solution snapshots) shock unsteadiness can be observed outboard of approximately 60% semi-span. Fluctuations in the shear layer downstream of the shock front are obvious between approximately 60% and 80% semi-span, coinciding both with the highest fluctuation levels along the shock front in the figure and the coherent flow structures of shock buffet based on unstable global modes described in [1, 2]. Overall, the two simulations give similar spatial extent of flow activity with some subtle differences in the detail.

Figure 6 presents the time history of the lift and drag coefficient for both simulations along with the power spectral density estimates of the lift coefficient for both the linear and non-linear part of the signal. The reader is reminded that the fluid-only simulation was started from the deeply converged static aeroelastic solution with the statically deformed aircraft geometry kept frozen. During the initial linear stage (up until approximately 0.015 s), the integrated coefficients appear to be independent of the structural degrees-of-freedom, specifically the signals of fluid-only and fluid-structure coupled simulations are very similar, and effectively follow the shock-buffet dynamics as described by the dominating global instability. Indeed, this initial growth of the lift coefficient in the fluid-structure coupled simulation, compared with the signal reconstructed from the leading unstable global modes identified in [2], can be found on the left in figure 7. Note that the non-linear time-marching solution will start deviating from the flow-field reconstruction based on a linear

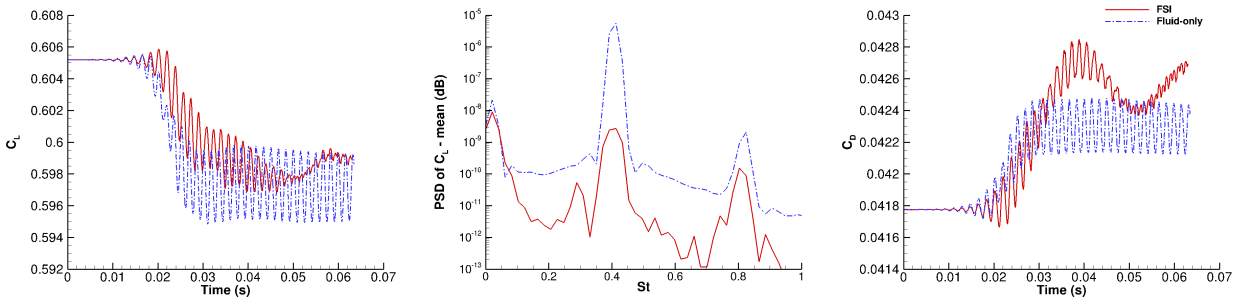

Fig. 6 Time history of unsteady lift (left) and drag coefficient (right) for both fluid-structure interaction (FSI) and fluid-only simulations and power spectral density (PSD) over Strouhal number for non-linear part (> 0.0305 s) of lift coefficient (middle).

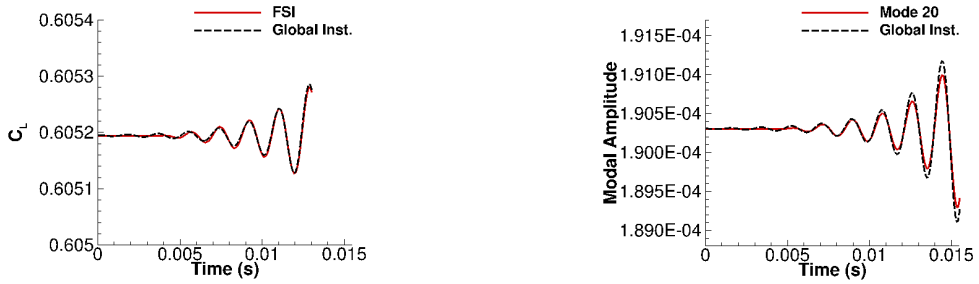

Fig. 7 Time response of lift coefficient for coupled the simulation (left) and modal amplitude of Mode 20 (right) along with signal based on leading unstable eigenvalue from global instability analysis in [2].

eigenmode, when the amplitudes exceed some case-dependent threshold. A similar agreement was found between the time-accurate fluid-only simulation and corresponding signal reconstructed from the global modes. In fact, the entire coupled fluid-structure system initially responds to the aerodynamic global instability, which effectively agrees with the classical aeroelastic approach when dealing with self-excited and self-sustained flow unsteadiness, i.e. to regard the aerodynamic forcing function independent of the structural motion. The corresponding structural response is visualised for mode 20, arbitrarily chosen as a representative example, showing the modal amplitude factor, $q(t)$, of that mode on the right in figure 7. The same behaviour is observed in all structural modes, as can partly be seen in figure 8, including the first bending modes even though not visible therein due to the strong non-linear signal.[†] Returning to figure 6, the non-linear part of the signal, here taken for time greater than 0.03 s, gives clear differences when including the flexible structure. First, the fluid-structure coupled solution results in lower-amplitude and more irregular instantaneous oscillations of the integrated coefficients. Second, the coupled results, besides the higher-frequency content, also reveal a low-frequency oscillation, possibly related to the dominant wing-bending deformation still present in the signal as visualised in figure 8. Third, the lift coefficient of the coupled simulation describes a slightly increased time-averaged response compared with the fluid-only simulation, as does the drag coefficient. The corresponding power spectral density estimates of the lift coefficient (with the corresponding frequency content for the drag coefficient appearing very similar) show strong peaks around the shock-buffet frequency range, as predicted by the global stability analyses [1, 2], and the first harmonic thereof. The fluid-structure coupled solution also gives a strong frequency activity, on a par with the magnitude of the shock-buffet peak, around the lowest structural modes.

Now that we have mentioned the unsteady modal structural amplitudes, $\boldsymbol{q}(t)$, on occasion, the discussion will now focus on those in more detail. Time histories of modal structural amplitudes for various different modes, corresponding to the modal shapes shown in figure 2, are presented in figure 8. Importantly, we include all structural modes that have been found to be unstable from the aeroelastic global stability analysis in our companion paper [2], specifically modes 19, 20, 21, 27 and 28. The linear part of the signals has already been discussed and the shock-buffet dynamics drive the response. Concerning the (more visible) non-linear part and from the unsteady signals shown in the figure, it is evident that the lower-frequency structural modes show little high-frequency content. The results of the characteristic higher-frequency shock-buffet forcing can be observed in the structural response for modes higher than, and including,

[†]There are two first bending modes at structural frequencies of 39.4 Hz and 40.9 Hz, with their modal shapes emphasising one wing each.

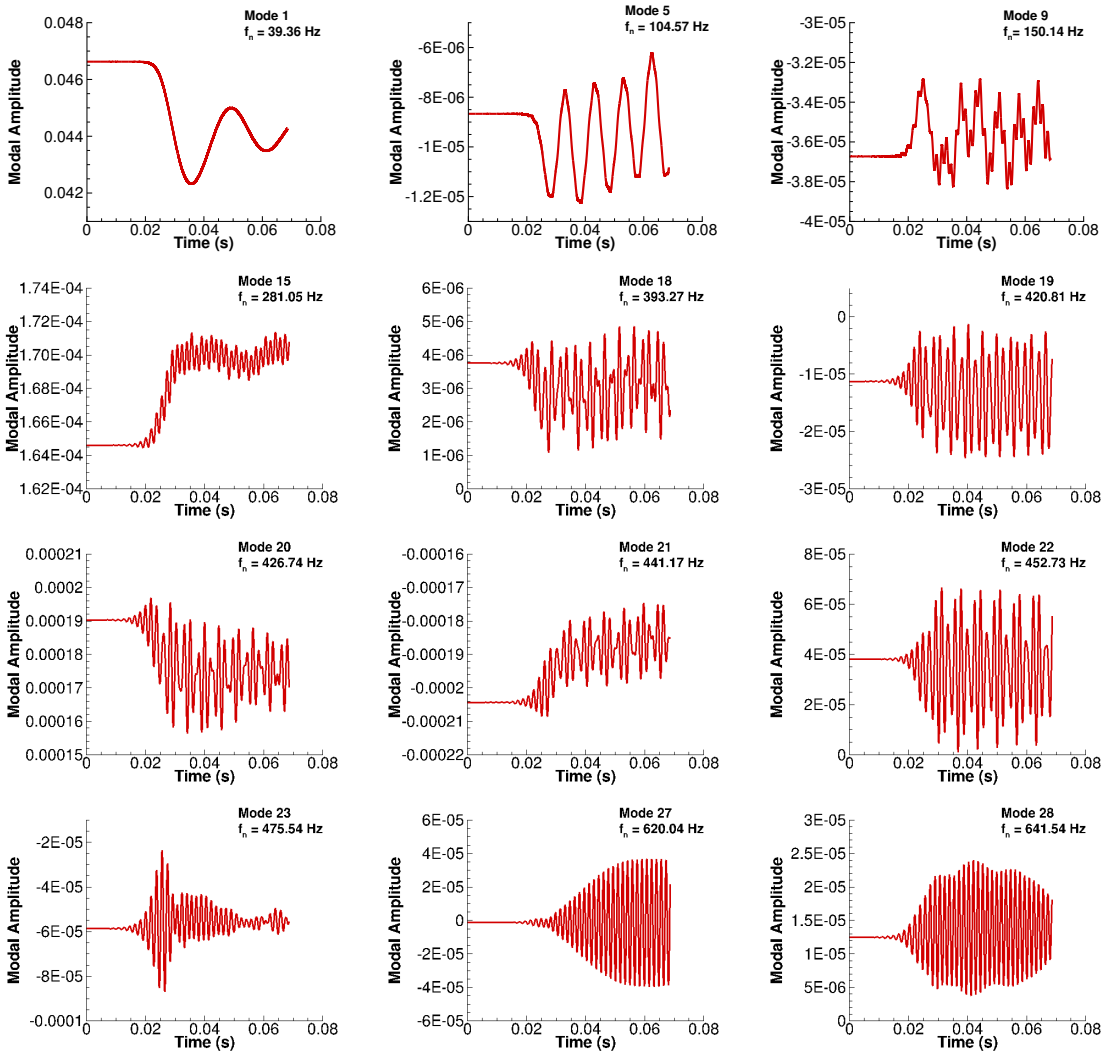

Fig. 8 Modal amplitude response for a few select modes of interest. The wind-off structural frequency of each mode is indicated. Modes 19, 20, 21, 27 and 28 have been found to be unstable following the global stability analysis of [2].

mode 9 with a wind-off structural frequency of $f_n \geq 150.14\,\text{Hz}$ (corresponding to a Strouhal number of approximately $St = 0.1$). In combination with figure 9, which presents the frequency content of the modal structural amplitudes, the time-domain signals reveal some additional interesting features. In particular, modes 27 and 28, which were found to be strongly coupled with a marginally unstable fluid mode (indeed, including the flexible wing structure destabilised the otherwise stable fluid mode in the first place) seem to oscillate at a single frequency. This is confirmed in figure 9 through the frequency content. The remaining structural modes, besides those with lowest wind-off frequencies where the vibration close to structural eigenmode dominates, all suggest more than one dominant frequency in their response. Overall, irregular limit-cycle oscillations can be observed in most modal amplitudes, hinting at the intense structural buffeting response of the wind-tunnel model at those flow conditions. What remains to be seen, when continuing the time-marching simulation, is the development of the first bending modes and the impact on the system dynamics.

Finally, figure 9 shows the frequency content of the modal structural amplitudes for each of the selected representative modes. The figure gives results for both the linear and non-linear part of the signal. Vertical lines indicate the Strouhal numbers of the respective wind-off structural frequencies and the frequency of the shock-buffet mode, as predicted by global stability analysis of the coupled system [2]. For the linear part, the signals show a single pronounced peak around the shock-buffet frequency. For the lower-frequency structural modes, activity can also be noted around the respective wind-off frequencies, which seems to be an artefact of choosing an appropriate time interval since the structural response

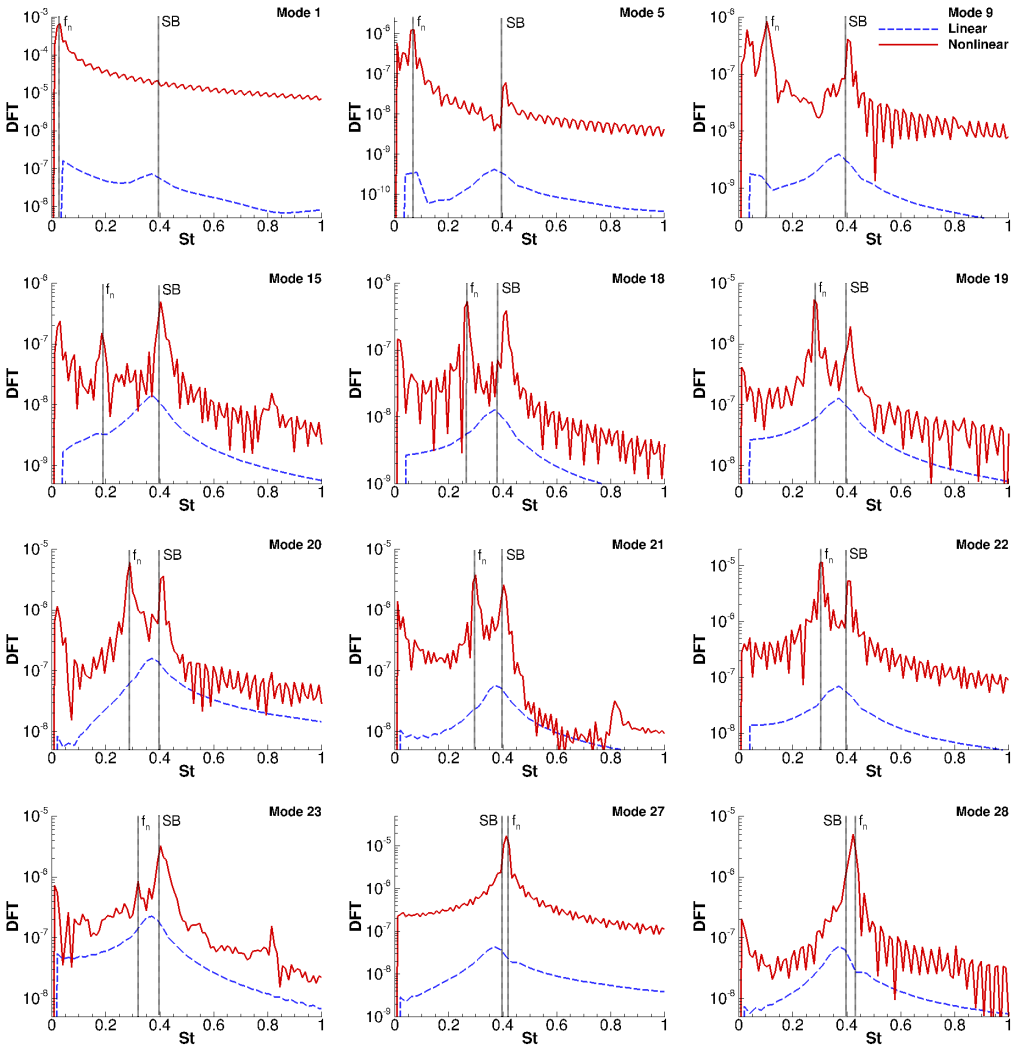

Fig. 9 Discrete Fourier transforms (DFT) of modal amplitudes of selected structural modes of interest for both linear and non-linear part of signal. Linear and non-linear limits of the time signal are considered at $t \leq 0.015$ s and $t \geq 0.03$ s, respectively. The frequency resolution for the linear and non-linear part is approximately $\Delta St = 0.03$ and 0.01, respectively. Vertical lines describe wind-off structural frequency, denoted f_n, and frequency of leading global shock-buffet mode (taken from [2]), denoted SB.

will eventually kick in. A different behaviour is revealed for the non-linear part altogether. Starting at mode 1 from the structural system, a single peak near its natural frequency is observed. As the structural frequencies increase, a mild peak around the shock-buffet frequency first appears for mode 5 while becoming more pronounced for modes 9 and above. A single strong peak near the shock-buffet frequency can be seen for the two highest frequency modes 27 and 28, whose wind-off frequencies are close to that of the flow instability. In addition to the responses related to either wind-off modal vibration or shock buffet, a relatively large response at the first bending modes can also be observed for most modes. The nature of this needs to be better understood from a longer, more settled time-marching simulation.

V. Conclusions

Unsteady fluid-structure coupled and fluid-only simulations for conditions beyond shock-buffet onset were carried out to investigate the dynamic interaction of a flexible aircraft model and self-sustained flow unsteadiness. While the fluid-structure coupled simulation requires longer run times still at the time of writing, first observations are reported herein. Basic validation of the static and time-averaged dynamic simulations with limited experimental data from a wind-tunnel experiment are reported with good agreement overall. Scrutinising both integrated force coefficients of lift

and drag and temporal amplitudes of the structural modes shows that the linear part of the signals is strongly dominated by the global shock-buffet instability, when started from a well converged static aeroelastic solution. In the non-linear regime, on the other hand, frequency content of the integrated coefficients becomes more broadband, revealing higher activity not only in the shock-buffet range but also near the first bending modes, with lower instantaneous oscillation amplitudes overall. The non-linear behaviour of the structural modes (strictly speaking, the interaction of the non-linear aerodynamic loads with the linear structural modes) strongly depends on their respective wind-off frequencies. For structural modes oscillating near the flow instability, a single strong peak is observed, in contrast to distinct peaks for structural vibration and flow instability for the more distant (in a frequency sense) structural modes.

Acknowledgments

The first author is grateful for the financial support received from Airbus. We also thank the University of Liverpool for computing time on the high-performance computer.

References

[1] Timme, S., "Global instability of wing shock-buffet onset," *Journal of Fluid Mechanics*, Vol. 885, 2020, p. A37. doi: 10.1017/jfm.2019.1001.

[2] Houtman, J., and Timme, S., "Towards Global Stability Analysis of Flexible Aircraft in Edge-of-the-Envelope Flow," *AIAA SciTech 2021 Forum*, 2021. AIAA 2021-xxxx.

[3] Hilton, W. F., and Fowler, R., *Photographs of shock wave movement*, HM Stationery Office, 1952.

[4] EASA, "Certification Specifications for Large Aeroplanes," Tech. rep., 2009.

[5] Jacquin, L., Molton, P., Deck, S., Maury, B., and Soulevant, D., "Experimental study of shock oscillation over a transonic supercritical profile," *AIAA Journal*, Vol. 47, No. 9, 2009, pp. 1985–1994.

[6] Garnier, E., and Deck, S., "Large-eddy simulation of transonic buffet over a supercritical airfoil," *Turbulence and Interactions*, Springer, 2010, pp. 135–141.

[7] Iovnovich, M., and Raveh, D. E., "Numerical study of shock buffet on three-dimensional wings," *AIAA Journal*, Vol. 53, No. 2, 2015, pp. 449–463.

[8] Banerjee, J., Liu, X., and Kassem, H., "Aeroelastic Stability Analysis of High Aspect Ratio Aircraft Wings," *Journal of Applied Nonlinear Dynamics*, Vol. 3, 2014, pp. 413–422.

[9] Crouch, J., Garbaruk, A., Magidov, D., and Travin, A., "Origin of transonic buffet on aerofoils," *Journal of Fluid Mechanics*, Vol. 628, 2009, pp. 357–369.

[10] Sartor, F., and Timme, S., "Reynolds-averaged Navier-Stokes simulations of shock buffet on half wing-body configuration," *53rd AIAA Aerospace Sciences Meeting*, 2015. AIAA 2016-1939.

[11] Timme, S., and Thormann, R., "Towards three-dimensional global stability analysis of transonic shock buffet," *AIAA Atmospheric Flight Mechanics Conference*, 2016. AIAA 2016-3848.

[12] Brunet, V., and Deck, S., "Zonal-detached eddy simulation of transonic buffet on a civil aircraft type configuration," *Advances in Hybrid RANS-LES Modelling*, Springer, 2008, pp. 182–191.

[13] Sartor, F., and Timme, S., "Delayed detached–eddy simulation of shock buffet on half wing–body configuration," *AIAA Journal*, Vol. 55, No. 4, 2016, pp. 1230–1240.

[14] Benoit, B., and Legrain, I., "Buffeting prediction for transport aircraft applications based on unsteady pressure measurements," *5th Applied Aerodynamics Conference*, 1987. AIAA 87-2356.

[15] Roos, F., "Surface pressure and wake flow fluctuations in a supercritical airfoil flowfield," *13th Aerospace Sciences Meeting*, 1975. AIAA 1975-66.

[16] McDevitt, J. B., and Okuno, A. F., "Static and dynamic pressure measurements on a NACA 0012 airfoil in the Ames high Reynolds number facility," Tech. rep., 1985.

[17] Lee, B., "Transonic buffet on a supercritical aerofoil," *The Aeronautical Journal*, Vol. 94, No. 935, 1990, pp. 143–152.

[18] Lawson, S., Greenwell, D., and Quinn, M. K., "Characterisation of buffet on a civil aircraft wing," *54th AIAA Aerospace Sciences Meeting*, 2016. AIAA 2016-1309.

[19] Masini, L., Timme, S., Ciarella, A., and Peace, A., "Influence of vane vortex generators on transonic wing buffet: further analysis of the BUCOLIC experimental dataset," *Proc. of the 52nd 3AF International Conf. on Applied Aerodynamics*, 2017.

[20] Blevins, R. D., *Flow-induced vibration*, Van Nostrand Reinhold Co., New York, 1977.

[21] Govardhan, R., and Williamson, C., "Resonance forever: existence of a critical mass and an infinite regime of resonance in vortex-induced vibration," *Journal of Fluid Mechanics*, Vol. 473, 2002, pp. 147–166.

[22] Raveh, D., and Dowell, E., "Frequency lock-in phenomenon for oscillating airfoils in buffeting flows," *Journal of Fluids and Structures*, Vol. 27, No. 1, 2011, pp. 89–104.

[23] Raveh, D. E., and Dowell, E. H., "Aeroelastic responses of elastically suspended airfoil systems in transonic buffeting flows," *AIAA Journal*, Vol. 52, No. 5, 2014, pp. 926–934.

[24] Quan, J., Zhang, W., Gao, C., and Ye, Z., "Characteristic analysis of lock-in for an elastically suspended airfoil in transonic buffet flow," *Chinese Journal of Aeronautics*, Vol. 29, No. 1, 2016, pp. 129–143.

[25] Gao, C., Zhang, W., Li, X., Liu, Y., Quan, J., Ye, Z., and Jiang, Y., "Mechanism of frequency lock-in in transonic buffeting flow," *Journal of Fluid Mechanics*, Vol. 818, 2017, pp. 528–561.

[26] Nitzsche, J., Ringel, L. M., Kaiser, C., and Hennings, H., "Fluid-mode flutter in plane transonic flows," *International Forum on Aeroelasticity and Structural Dynamics*, 2019.

[27] Steimle, P. C., Karhoff, D.-C., and Schröder, W., "Unsteady transonic flow over a transport-type swept wing," *AIAA Journal*, Vol. 50, No. 2, 2012, pp. 399–415.

[28] Masini, L., Timme, S., and Peace, A., "Analysis of a civil aircraft wing transonic shock buffet experiment," *Journal of Fluid Mechanics*, Vol. 884, 2020, p. A1.

[29] Belesiotis-Kataras, P., and Timme, S., "Harmonic Forcing Amplitude Effects in Globally Unstable Transonic Wing Flow," *AIAA SciTech 2020 Forum*, 2020. AIAA 2020-1985.

[30] Vassberg, J., DeHaan, M., Rivers, M., and Wahls, R., "Development of a common research model for applied CFD validation studies," *26th AIAA Applied Aerodynamics Conference*, 2008. AIAA 2008-6919.

[31] Belesiotis Kataras, P., and Timme, S., "Numerical study of incipient transonic shock buffet on large civil aircraft wings," *Royal Aeronautical Society 2018 Applied Aerodynamics Conference*, 2018.

[32] Meinel, M., and Einarsson, G. O., "The FlowSimulator framework for massively parallel CFD applications," *PARA 2010*, 2010.

[33] Keye, S., and Gammon, M. R., "Development of Deformed Computer-Aided Design Geometries for the Sixth Drag Prediction Workshop," *Journal of Aircraft*, Vol. 55, No. 4, 2018, pp. 1401–1405. doi:10.2514/1.C034428.

[34] Tinoco, E. N., Brodersen, O. P., Keye, S., Laflin, K. R., Feltrop, E., Vassberg, J. C., Mani, M., Rider, B., Wahls, R. A., Morrison, J. H., Hue, D., Roy, C. J., Mavriplis, D. J., and Murayama, M., "Summary Data from the Sixth AIAA CFD Drag Prediction Workshop: CRM Cases," *Journal of Aircraft*, Vol. 55, No. 4, 2018, pp. 1352–1379. doi:10.2514/1.C034409.